First-principles simulations of intrinsic collision cascades of 23-eV/amu Si and 5-eV/amu Ti atoms in single-crystal Si and Ti

A. Kuronen
Accelerator Laboratory, University of Helsinki,
P.O. Box 43 (Hämeentie 100), FIN-00014 Helsinki, Finland
and Research Institute for Theoretical Physics, University of Helsinki,
P.O. Box 9 (Siltavuorenpenger 20C), FIN-00014 Helsinki, Finland

J. Keinonen
Accelerator Laboratory, University of Helsinki,
P.O. Box 43 (Hämeentie 100), FIN-00014 Helsinki, Finland

K. Kaski
Research Institute for Theoretical Physics, University of Helsinki,
P.O. Box 9, (Siltavuorenpenger 20C), FIN-00014 Helsinki, Finland
and Tampere University of Technology, P.O. Box 692, FIN-33101 Tampere, Finland
(Received 12 August 1993)

The slowing-down process of Ti atoms in crystalline Ti and Si atoms in crystalline Si is studied using the molecular-dynamics method. Based on an experimental technique available for studies of the slowing-down process of atoms at ultralow velocities in bulk matter, the initial recoil energy was 261 eV for Ti and 677 eV for Si atoms. The values correspond to the energies imparted after the thermal neutron capture by primary γ rays. The effect of the crystalline structure on the slowing-down process is studied by calculating the energy distribution of the Doppler-shifted secondary γ rays emitted by the recoiling nuclei. The dependence of the distribution on the interatomic potential used in the simulations is also investigated.

I. INTRODUCTION

A recently developed experimental method at the Institut Laue Langevin (ILL) to measure lifetimes of excited nuclear states,[1,2] makes it possible to study interatomic collisions in a bulk matter at ultralow velocities, i.e., from 10^5 m/s down to thermal velocities of about 10^3 m/s. In this γ-ray-induced Doppler broadening (GRID) method, the emission of a primary γ ray from the compound nucleus as a result of the thermal neutron capture reaction produces an excited nucleus that recoils at energies of few hundred eV. Subsequent secondary γ rays emitted by the excited nucleus of the recoiling atom are Doppler shifted. This shift depends on the lifetime of the excited nuclear state emitting the secondary γ rays and on the slowing-down time of the recoiling atom.[3] The unique energy resolution of the two axes flat double crystal γ spectrometer GAMS4 installed at ILL makes it possible to observe the broadening of the γ-ray line shapes, which originate from the Doppler shifts.[4,5]

In order to simulate experimental GRID data, modeling of the interatomic collisions between the recoiling atom and the lattice atoms is required. Because of the low recoil energies involved in the GRID method, calculation of the slowing-down process using the binary collision approximation[6] (BCA) is not sufficiently reliable and accurate for comparison with the experimental data. The most realistic way to calculate the slowing down at these low energies is the molecular dynamics (MD) method.[7,8] Previously such MD simulations have been performed in connection with GRID to obtain nuclear lifetimes[9] and to study the interatomic potentials responsible for the slowing-down process.[10]

So far GRID measurements have been made with polycrystalline or powder targets only. This means that the angular information from the slowing-down process is smeared out from the GRID γ-ray line shape. Until now it has been possible to extract only one parameter from the line shape, namely the nuclear lifetime or the average slowing-down time of the recoil. However, by using monocrystalline targets, the orientation of the target crystal relative to the target-detector axis remains fixed and thus there will be some fine structure in the line shapes. To study such effects, some preliminary MD simulations of GRID line shapes for slowing down of Si atoms in monocrystalline silicon have been performed very recently.[11]

In this work we use MD simulations to study the effect of the crystalline structure on the GRID γ-ray line shape and on the slowing-down process of few hundred eV recoils. The effect of the interatomic potential is also studied. For the simulations we have chosen two cases that can be studied experimentally with the GRID technique. First we study the interatomic collisions in the tightly packed hcp lattice structure of Ti [Fig. 1(a)], fo-

0163-1829/94/49(6)/3766(8)/$06.00

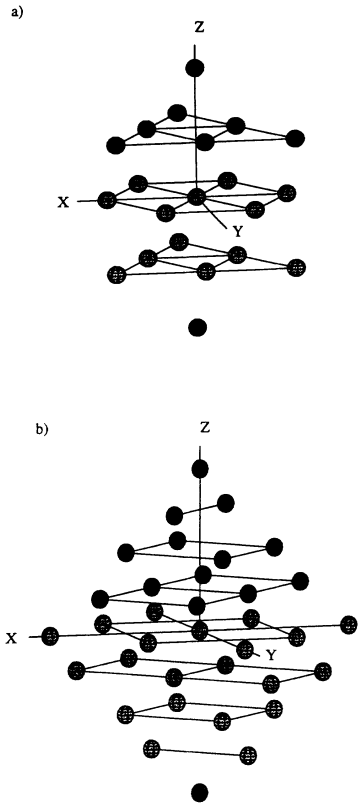

FIG. 1. (a) Nearest neighbors in the hcp lattice. Due to the different environments of successive layers the other sublattice can be formed by rotating the figure around the z axis through 60°. (b) Nearest neighbors in the diamond lattice. The other sublattice can be formed by rotating the figure around the z axis through 90°.

cusing on the slowing down of ^{49}Ti recoils as produced in the reaction $^{48}\mathrm{Ti}(n,\gamma)^{49}\mathrm{Ti}$. The γ transition from the 8.14-MeV capturing state to the 3.26-MeV state produces a recoil energy of 261 eV. The γ-ray line to be observed is emitted from the 1499-keV transition 3.26 $\rightarrow$ 1.76 MeV. This cascade was chosen because the 3.26-MeV level has a suitably short lifetime [16.2 ± 0.7 fs (Ref. 9)] and is predominantly populated directly from the capturing state at 8.14 MeV.[12] Second, we study the slowing down of ^{29}Si recoils in the open diamond lattice structure of Si [Fig. 1(b)], as produced in the reaction $^{28}\mathrm{Si}(n,\gamma)^{29}\mathrm{Si}$. In this case the γ transition from the 8.47-MeV capturing state to the 2.43-MeV state results in a recoil energy of 677 eV. The γ line to be observed corresponds to the transition 2.43 $\rightarrow$ 0 MeV. The lifetime of the 2.43-MeV level is 26.6 ± 1.6 fs (Ref. 13) and it is predominantly populated directly from the capturing state.[14]

This paper is organized so that we first discuss the principles of simulating the slowing-down process, Sec. II. Then the calculations of the GRID line shapes for monocrystalline samples are described briefly, Sec. III. The simulation results are presented in Sec. IV and conclusions are drawn in Sec. V.

II. PRINCIPLES OF MOLECULAR-DYNAMICS SIMULATIONS

The MD simulation method used in this work is to a large extent the same as the one used in Ref. 9, i.e., constant volume and energy calculations. The positions and velocities of an ensemble of atoms are calculated by numerically integrating classical Newton's equations of motion

$$\frac{d\mathbf{r}_i}{dt} = \mathbf{v}_i, \tag{1}$$

$$\frac{d(m_i\mathbf{v}_i)}{dt} = \sum_{j\neq i} \mathbf{F}(r_{ij}). \tag{2}$$

Here $\mathbf{r}_i$, $\mathbf{v}_i$, and m_i are the position, velocity, and mass of atom i, respectively, and

$$\mathbf{F}(r_{ij}) = -\left[\frac{dV(r)}{dr}\right]_{r=r_{ij}} \frac{\mathbf{r}_{ij}}{r_{ij}} \tag{3}$$

is the force of atom j on atom i, derived from the interatomic pair potential $V(r)$. The numerical scheme of integration in Eqs. (1) and (2) is the variable time step algorithm by Smith and Harrison:[15]

$$\mathbf{r}_{i,n+1} = \mathbf{r}_{i,n} + \mathbf{v}_{i,n}\Delta t_n + [(3+R)\mathbf{a}_{i,n} - R\mathbf{a}_{i,n-1}]\frac{\Delta t_n^2}{6}, \tag{4}$$

$$\mathbf{v}_{i,n+1} = \mathbf{v}_{i,n} + \left(\frac{3+2R}{1+R}\mathbf{a}_{i,n+1} + (3+R)\mathbf{a}_{i,n} - \frac{R^2}{1+R}\mathbf{a}_{i,n-1}\right)\frac{\Delta t_n}{6}, \tag{5}$$

where $\mathbf{r}_{i,n}$, $\mathbf{v}_{i,n}$ and $\mathbf{a}_{i,n}$ are the position, velocity, and acceleration of particle i, respectively, at time step n with magnitude Δt_n, and $R = \Delta t_n/\Delta t_{n-1}$. Due to the change in the velocities of atoms by about 1 order of magnitude during the simulation of the slowing-down process, the variable time step algorithm was used to minimize the computing time. In the simulations, the initial values, $\Delta t_0 = 0.5$ fs for Ti and 0.25 fs for Si were chosen, which for a recoiling atom at the initial velocity correspond to a traveled distance of 0.16 Å. For each time step n a particle with the largest velocity in the system was searched. If it moved less than 0.1 Å during Δt_n and if its velocity was less than five times the thermal velocity, time Δt_0 was added to Δt_n. Periodic boundary conditions were applied in all three dimensions of the simulation cell. When the periodic boundary conditions are used in the simulations of the slowing-down process of a high-energy recoil, it must be assured that the recoiling atom does not experience the damage it has created. Therefore, the MD cell has to be so large that the energy due to the recoil process cannot traverse across the MD cell within the simulation time. A cell of 900 atoms with dimensions 26.6 × 25.5 × 23.5 Å^3 was found sufficient for

Ti. Also some test runs were done with a cell of 1848 atoms ($32.5 \times 30.7 \times 32.8$ Å^3), yielding results without any significant difference compared with those obtained with the smaller cell. The cell size for the simulation with the Si was 1000 atoms ($27.2 \times 27.2 \times 27.2$ Å^3). Due to fairly large MD cells and simulation times of 200 fs, no temperature correction was needed during the simulations.

The high-energy part of the interaction between Ti atoms was described by the repulsive pair potential, calculated with the effective medium theory (EMT) (see Ref. 8 and references therein). The right crystal structure and lattice constant of Ti was obtained by splining the Morse potential of Ref. 16 between $r = 2.0$ and 2.5 Å with the repulsive potential. In the case of Si the repulsive interaction between atoms was described by the potential calculated using the DMol package.[17] The attractive interaction between Si atoms was described by the pair potential of Ref. 18. This yields the right diamond structure of the crystalline Si. In this case the potential was splined between $r = 1.7$ and 2.0 Å with the repulsive potential. Because of the recoil energies of few hundred eV only the repulsive part of the potential is significant and there is no need to use many-body potentials which would require more computing time than pair potentials. On the other hand, the recoil energies are so low that simultaneous collisions of the recoiling atom from the repulsive potentials of more than one lattice atom at a time affect the slowing down of the recoil, thus excluding the use of BCA in this case. In order to test the effect of a different interatomic potential we also used the universal repulsive potential of Ziegler *et al.*[19] (ZBL) which has been widely adopted for computer simulations of slowing down of energetic ions. The repulsive potentials for the Ti-Ti and Si-Si interactions are shown in Fig. 2. In some test simulations the electronic energy loss[19] was found to be negligible for the considered recoils and was therefore not included in the simulations.

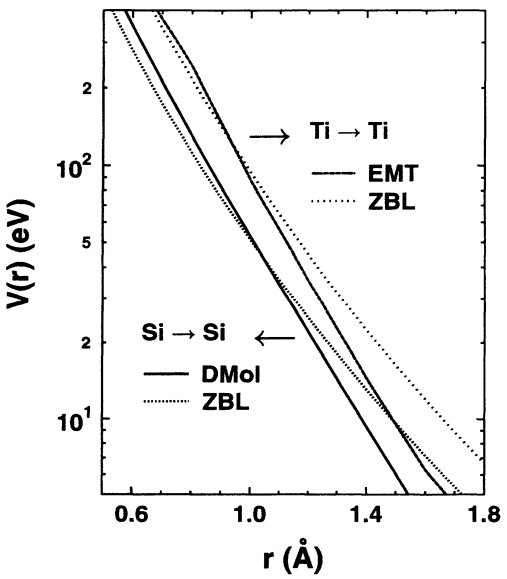

FIG. 2. Repulsive pair potentials for the Ti-Ti and Si-Si interactions used in the MD simulations.

Before initiating a recoil event atoms in their lattice sites were given a random thermal velocity that corresponds to the appropriate Maxwell distribution. Then the system was equilibriated by simulating it undisturbed for 1 ps. In this way the effects of the finite temperature through thermal displacement of lattice atoms was included in the model. In both the Ti and Si simulations the temperature was set to 300 K. After this the recoil velocity was imparted to one of the atoms in random direction corresponding to the isotropic distribution of the primary γ rays. The slowing down of the recoil was then calculated up to 200 fs. In order to get sufficient statistics for the calculation of the γ-ray line shapes, about 6000 recoil events were simulated for both Ti and Si systems. We now move to discuss the calculation of GRID line shapes for single-crystal samples.

III. CALCULATION OF GRID LINE SHAPES

In the case of polycrystalline targets, the GRID line shapes have recently been calculated from the velocity distribution of the recoiling atom.[9] However, for monocrystalline targets the angular information of the recoil velocity is required. In the simulations, the velocity vector of the recoiling atom $\mathbf{v}_i(t)$ was stored for every recoil event at every time step. The γ-ray line shape corresponding to the mean lifetime τ of the excited nuclear state is then calculated from these velocities by generating a lifetime t' with a Poisson probability distribution

$$P = e^{-t'/\tau} \tag{6}$$

for each recoil event i. The energy of the emitted γ quantum is

$$E = E_0 \left(\frac{\mathbf{v}_i(t') \cdot \mathbf{n}}{c} + 1 \right), \tag{7}$$

where E_0 is the unshifted γ energy, $\mathbf{n}$ is a unit vector in the direction of the detector, and c is the speed of light in vacuum. In the calculation of the line shape for a polycrystalline sample, the direction of the detector is generated randomly for every recoil event. This is equivalent to a situation where every recoiling atom slows down in a randomly oriented single crystal.[8–10] Now we are ready to describe the actual simulation results.

IV. RESULTS AND DISCUSSION

A. Angular distribution of velocity vectors

In Figs. 3 and 4 we show the distribution of the recoil velocity directions for atoms leaving a lattice site at different times. The recoil energies are 261 eV and 677 eV for Ti and Si atoms, respectively. One can clearly see the effect of the lattice structure on the angular distribution of the velocity vectors $\mathbf{v}_i(t)$ [Eq. (7)] and thus on the slowing-down process.

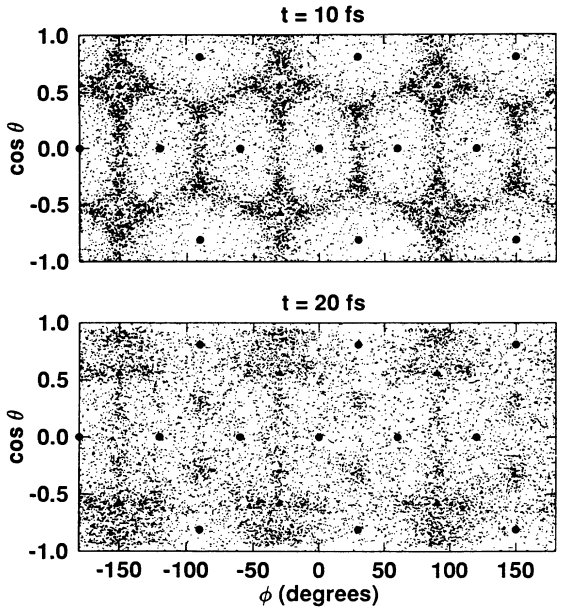

FIG. 3. Simulated angular distribution of the recoil velocities of ^{49}Ti atoms recoiling in single-crystal Ti 10 and 20 fs after the start of the recoil event. The recoiling atom was always from the same sublattice of the hcp structure. The directions of the nearest (circles) and second-nearest (triangles) neighbors are shown. The other sublattice results can be formed by shifting the pattern 60° along the ϕ axis. The EMT potential was used in the simulation.

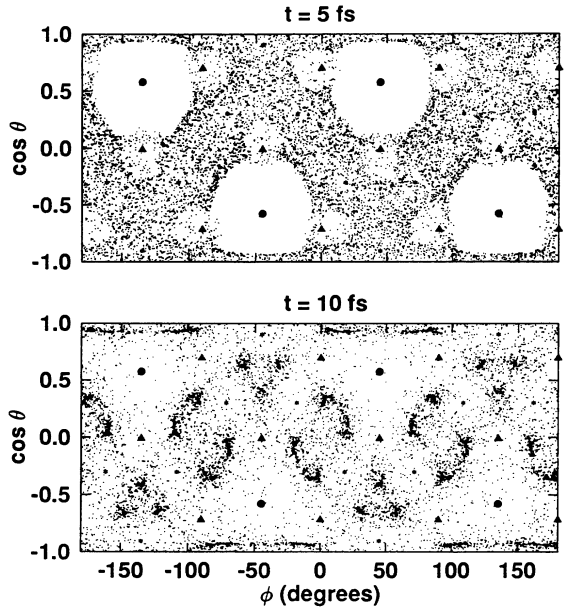

FIG. 4. Simulated angular distribution of the recoil velocities of ^{29}Si atoms recoiling in single-crystal Si 5 and 10 fs after the start of the recoil event. The recoiling atom was always from the same sublattice of the diamond structure. Also shown are the directions of the nearest (circles), second-nearest (triangles), and third-nearest (asterisks) neighbors. The other sublattice results can be obtained by shifting the pattern 90° along the ϕ axis. The DMol potential was used in the simulation.

In the case of Ti the focusing effect of the lattice was found to be most pronounced at 10 fs after the start of the recoil event (Fig. 3). This is in contrast with the behavior for times either shorter than 5 fs or longer than 20 fs, when the angular distribution of recoils appears isotropic. For short times this happens because hardly any recoiling atom collisions from lattice atoms take place. However, for long times the recoils experience so numerous multiple collisions, that no clearly preferable focusing directions can any longer be seen in the recoil velocity distribution. Also the thermal displacement of lattice atoms diminishes the focusing effects. Nevertheless, the effect of the crystal structure on the slowing-down process of a single recoil does exist at all times. The triangle- and square-shaped focusing lenses formed by the nearest neighbors [Fig. 1(a)] focus the recoiling atoms into directions $\phi = -150°, -30°, 90°; \cos\theta = \pm 0.33$ and

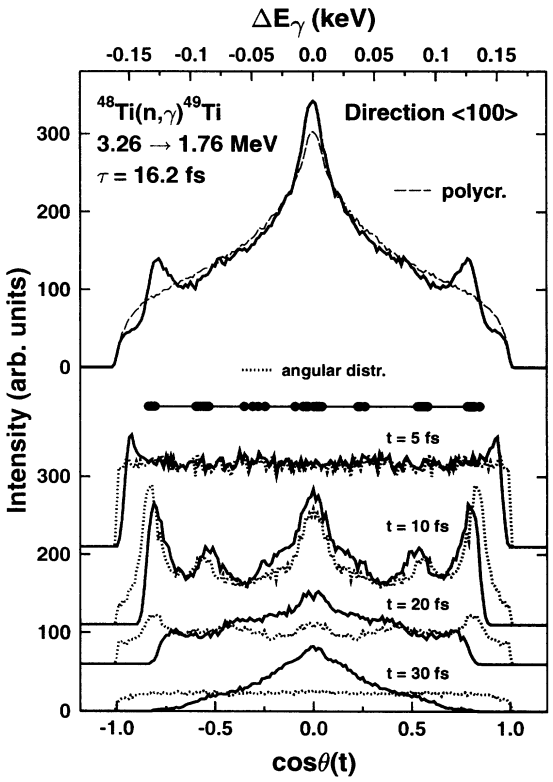

FIG. 5. The lower part shows projections of angular distributions of the velocity of recoiling Ti atoms, $\cos\theta(t)$ (dashed line) and corresponding energy distributions when the slowing down is taken into account, ΔE_γ (solid line) at different times after the initiation of the recoil event. The intensities of the angular distributions at different times have been scaled by the exponential decay law [Eq. (6)] using 16.2 fs as the mean lifetime. In the upper part the actual line shape of the secondary γ ray is shown assuming a single-crystal sample and the detector placed in the $\langle 100 \rangle$ direction and the mean lifetime 16.2 fs of the nuclear level emitting the γ ray (solid line). Also shown is the line shape obtained by assuming a polycrystalline target (dashed line). Circles on the horizontal line in the middle of the figure show the projections corresponding to the directions of the maxima in the angular distribution at $t = 10$ fs. The EMT potential was used in the simulation.

$\phi = -90°, 30°, 150°; \cos\theta = \pm 0.57$, respectively, where ϕ is the angle between the velocity vector $\mathbf{v}_i(t)$ and the x axis in the xy plane shown in Fig. 1(a) and θ is the angle between $\mathbf{v}_i(t)$ and z axis. The corresponding numbers for the recoils from the other sublattice of the hcp structure can be obtained by adding 60° to the ϕ values given above. The second-nearest neighbors in the direction of the square-shaped lens [Fig. 1(a)] cause the maxima in the angular distribution in this direction to split into four.

In Si the focusing effect of the lattice was found to be most pronounced at 5 fs after the start of the recoil event (Fig. 4). This happens when the recoiling atom has collided with its nearest neighbors [Fig. 1(b)]. At 10 fs the scattering of the recoiling atoms from their second-nearest neighbors changes the distribution strongly. In this case the angular distributions were found isotropic for times shorter than 2 fs and longer than 20 fs. This happens exactly for the same reason as in the case of Ti. The focusing lenses formed by nearest and second-nearest neighbors focus the recoiling atoms into following directions $\phi = 168°, \cos\theta = -0.95$; $103, -0.95$; $14, 0.95$; $80, 0.95$; $60, -0.65$; $32, -0.65$; $122, 0.65$; $150, 0.65$; $45, -0.42$; $135, 0.42$; $175, -0.34$; $97, -0.34$; $5, 0.34$; $85, 0.34$; $160, -0.09$; $112, -0.09$; $20, 0.09$; and $71, 0.09$. Due to the symmetry of the diamond structure in silicon, maxima can also be found in directions obtained from the above values by changing the signs. The corresponding numbers for the recoils from the other sublattice of the diamond structure can be obtained by adding 90° to the ϕ values given above.

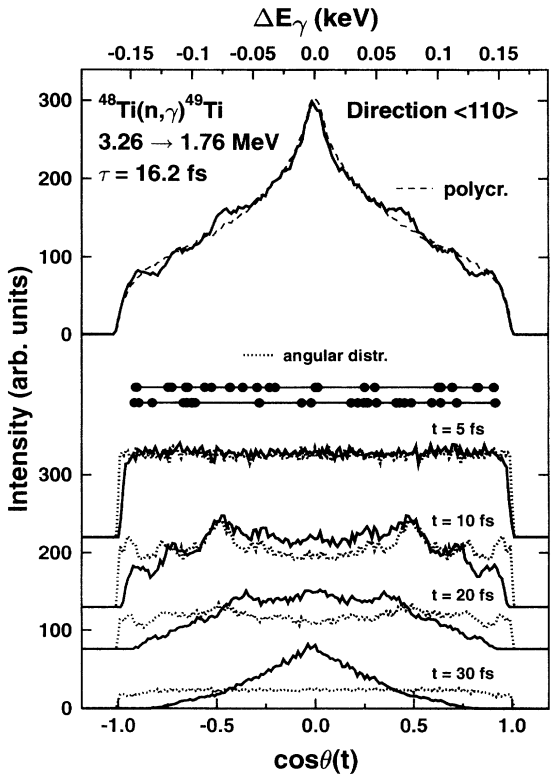

FIG. 6. As for Fig. 5, but for the ⟨110⟩ direction.

B. Gamma-ray line shape for Ti

The projections of the angular distributions shown in Fig. 3 are given in Figs. 5, 6, and 7 in the ⟨100⟩, ⟨110⟩, and ⟨001⟩ directions, respectively. They are shown as a function of $\cos\theta(t)$, where $\theta(t)$ is the angle between the ⟨100⟩, ⟨110⟩, or ⟨001⟩ directions and $\mathbf{v}_i(t)$ at time t. The focusing effect at $t = 10$ and 20 fs and the isotropy of the angular distribution at $t = 5$ and 30 fs are well demonstrated. The distributions correspond to the γ-ray line shapes that are calculated for the specific times without taking into account the exponential distribution [Eq. (6)] of γ-ray emission times (except in the scaling of the intensities of the distributions) and slowing down, i.e., decrease of the recoil velocity. The projections of the focusing directions are illustrated by the filled circles on the horizontal line in the middle of Figs. 5, 6, and 7.

In the ⟨100⟩ direction, the focusing effect is observable as strong maxima at $\cos\theta(t = 10\text{ fs}) = 0, \pm 0.55$, and ± 0.85 corresponding to the Doppler shifts of $\Delta E_\gamma = 0, \pm 0.090$, and ± 0.135 keV, respectively. The effect of the slowing down on the Doppler shift is also shown for different projections of the angular distributions. These maxima at ± 0.090 and ± 0.135 are shifted to smaller values of ± 0.085 and ± 0.130 keV, respectively. When the real γ-ray line shape is calculated by summing the distributions at different times and weighting by the Poisson distribution,

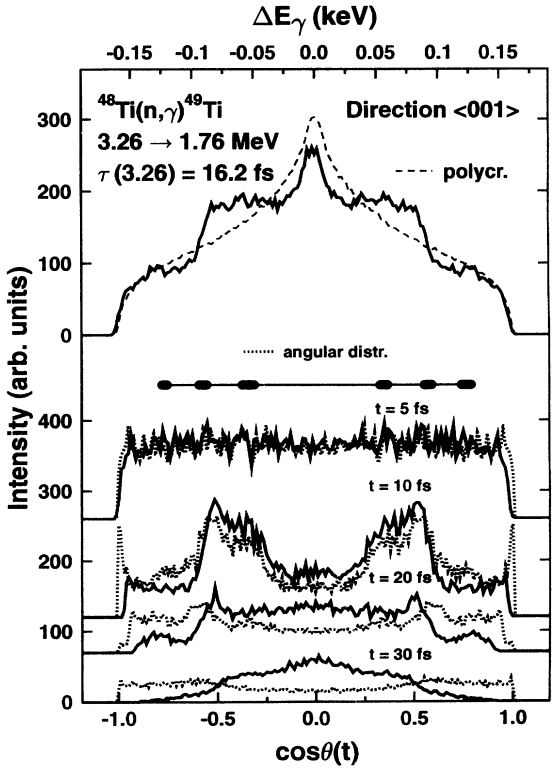

FIG. 7. As for Fig. 5, but for the ⟨001⟩ direction.

$\exp(-t/\tau)$ the line shape shown also in Fig. 5 is obtained. The strong peaks at $\Delta E_\gamma = \pm 0.130$ keV are still clearly observable. To demonstrate the significance of the focusing effects, we have also simulated the line shape of the 3.26 $\rightarrow$ 1.76 MeV transition in a polycrystalline Ti sample.

When the detector is placed in the $\langle 110 \rangle$ direction the lattice structure is such that there are several projections of the focusing directions as shown in the middle of Fig. 6. The projections of the maxima in the angular distribution (filled circles in Fig. 6) are evenly distributed on the $\cos\theta(t)$ axis. In the line shape they appear as weak and broad maxima at the Doppler shifts of $\Delta E_\gamma = \pm 0.110$, ± 0.075, and ± 0.145 keV when compared with the line shape calculated for the polycrystalline sample.

In the $\langle 001 \rangle$ direction there are two strong and broad maxima around ± 0.075 keV and weaker and narrower ones at ± 0.125 keV. This can be understood by observing that the maxima in the angular distribution are gathered into six groups on the $\cos\theta(t)$ axis, namely at $\pm 0.34, \pm 0.56$, and ± 0.77 when the projection is taken in the $\langle 001 \rangle$ direction. In comparison with the line shape calculated for the polycrystalline target, this structure in the γ-ray line is very pronounced.

C. Gamma-ray line shapes for Si

In Figs. 8, 9, and 10 the projections of angular distributions of Fig. 4 are given in the $\langle 100 \rangle$, $\langle 110 \rangle$, and $\langle 111 \rangle$

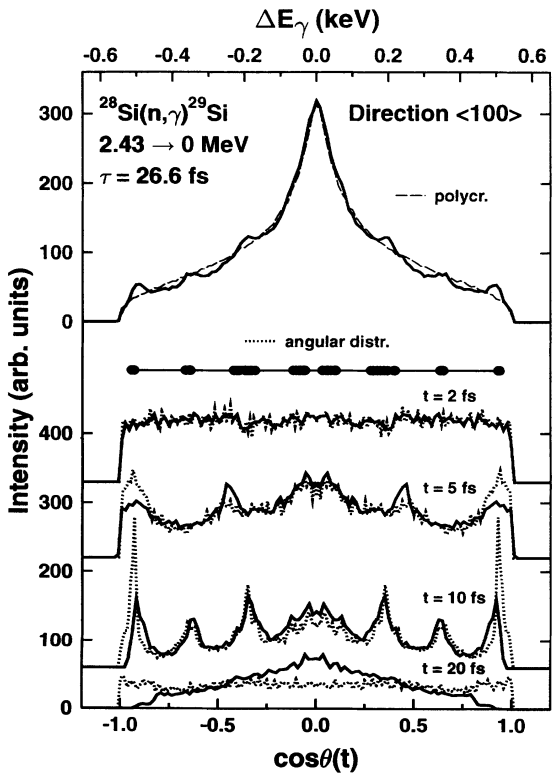

FIG. 8. As for Fig. 5, but for recoiling Si atoms in c-Si. The lifetime of the nuclear level emitting the γ ray was 26.6 fs. The DMol potential was used in the simulation.

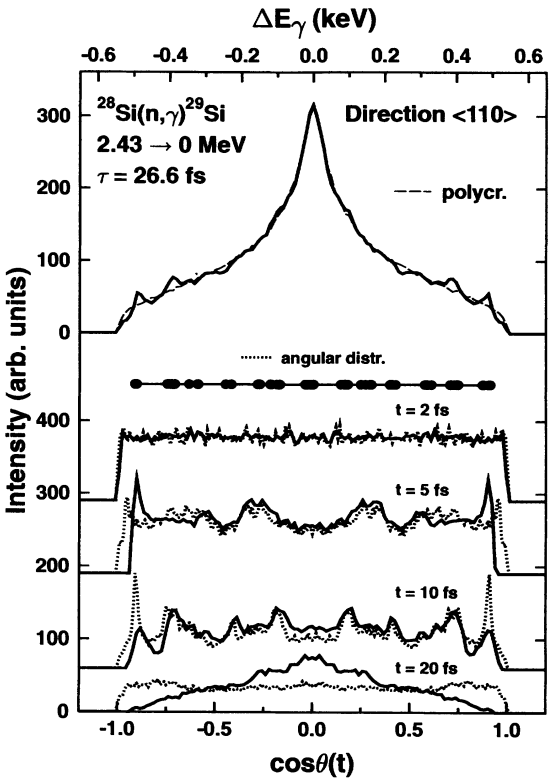

FIG. 9. As for Fig. 8, but for the $\langle 110 \rangle$ direction.

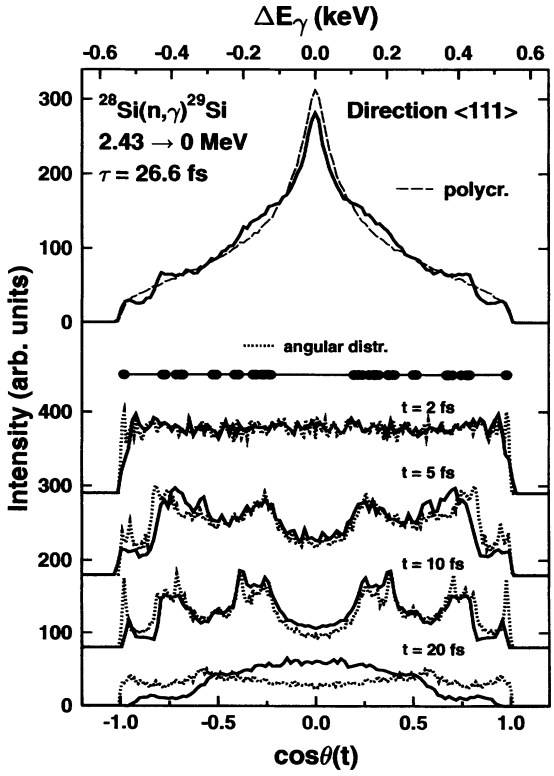

FIG. 10. As for Fig. 8, but for the $\langle 111 \rangle$ direction.

directions, respectively. They are shown as a function of $\cos\theta(t)$, where $\theta(t)$ is now the angle between the $\langle 100\rangle$, $\langle 110\rangle$, or $\langle 111\rangle$ directions, and $\mathbf{v}_i(t)$. The focusing effect at $t = 5$ and 10 fs and the isotropy of the angular distribution at $t = 2$ and 20 fs are well demonstrated. These distributions correspond to the γ-ray line shapes calculated for specific times, without taking into account the slowing down and the exponential distribution in the γ-ray emission times (except in the scaling of the intensities of the distributions). The projections in the focusing directions are illustrated by the filled circles on the horizontal line in the middle of Figs. 8, 9, and 10.

In the $\langle 100\rangle$ direction, the maxima in the angular distribution (Fig. 4) are grouped into seven peaks (filled circles in Fig. 8) at $\cos\theta(t = 10\text{ fs})$=0, ± 0.36, ± 0.65, and ± 0.93. These values correspond to the Doppler shifts of $\Delta E_\gamma = 0$, ± 0.20, ± 0.35, and ± 0.51 keV. We have also shown the effect of the slowing down on the Doppler shift for different angular distributions. The maxima at ± 0.20, ± 0.35, and ± 0.51 keV are shifted to the smaller values of ± 0.19, ± 0.34, and ± 0.49 keV, respectively. When the real γ-ray line shape is calculated by summing distributions at different times and weighting by $\exp(-t/\tau)$ the line shape in Fig. 8 is obtained. The comparison with the line shape of the 2.43 $\rightarrow$ 0 MeV transition for a polycrystalline slowing down medium shows that the strong peaks at $\Delta E_\gamma = \pm 0.18$, ± 0.34, and ± 0.49 keV are still clearly observable.

When the detector is placed in the $\langle 110\rangle$ direction the lattice structure yields so many projections of the focusing directions that there are no strong separate focusing effects in this direction as shown in the middle of Fig. 9. The projected maxima in the angular distribution are evenly distributed on the $\cos\theta(t)$ axis (filled circles in Fig. 9). However, some of the maxima are strong enough to show fine structure in the simulated γ-ray line shape at the Doppler shifts of ± 0.39 and ± 0.49 keV.

In the $\langle 111\rangle$ direction there are four broad peaks around ± 0.18 and ± 0.43, and a narrower one at ± 0.52 keV. This can be understood from the projected maxima in the angular distribution (filled circles in Fig. 10) which are grouped into six groups on the $\cos\theta(t)$ axis. The line shape deviates clearly from the one simulated with a polycrystalline sample.

D. Effect of interatomic potential

First of all we point out that changing the EMT potential for Ti to the more repulsive ZBL potential[19] will move the Doppler-shifted peaks in the line shape to smaller energy values. This is caused by the larger energy loss in the focusing lenses (Fig. 11) of the crystalline structure. This phenomenon is most clearly seen for the $\langle 100\rangle$ direction where the peaks at ± 0.130 keV are shifted to ± 0.120 keV. The intensity at zero Doppler shift is also increased due to the reduction in the slowing-down time. It is worth noting that the relative positions of the peaks simulated with the two different potentials remained the same when the lifetime value of the 3.26-MeV state was varied. This was also checked by trying to fit the $\langle 100\rangle$

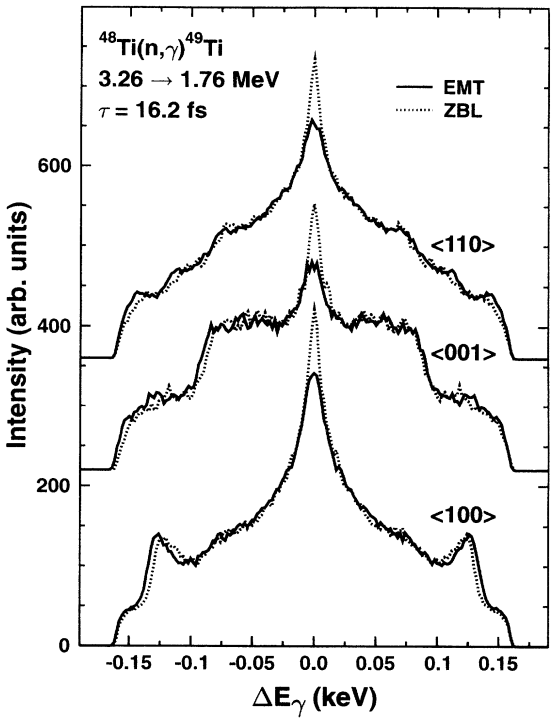

FIG. 11. Simulated GRID line shapes for Ti. The detector was in the $\langle 100\rangle$, $\langle 001\rangle$, and $\langle 110\rangle$ directions. The EMT (solid line) and ZBL (dashed line) potentials were used in the simulations. The lifetime of the 3.26-MeV state in ^{49}Ti was 16.2 fs.

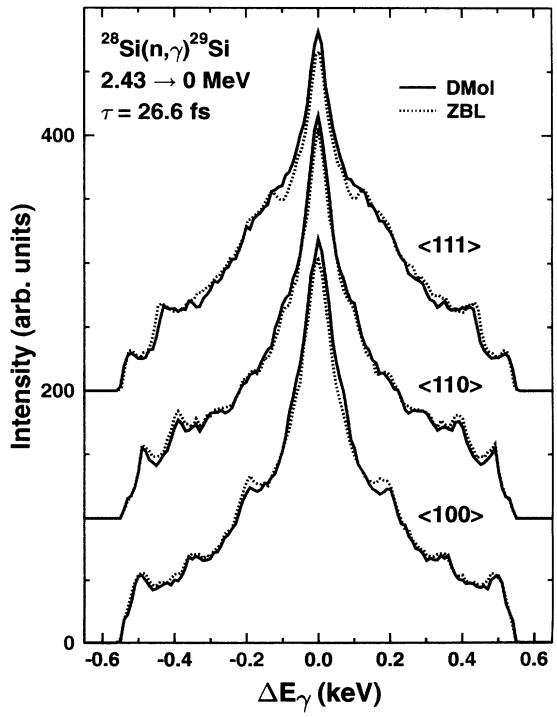

FIG. 12. Simulated GRID line shapes for Si. The detector was in the $\langle 100\rangle$, $\langle 110\rangle$, and $\langle 111\rangle$ directions. The DMol (solid line) and ZBL (dashed line) potentials were used in the simulations. The lifetime of the 2.43-MeV state in ^{29}Si was 26.6 fs.

line shape calculated using the ZBL potential to the line shape calculated with the EMT potential. However, no satisfactory fit was obtained by varying the lifetime in the line shape simulations with the ZBL potential. Thus the lifetime and the interatomic potential affect the line shape in different ways. Although it is in principle possible to determine both the lifetime and the interatomic potential from the same GRID line shape, the differences in Figs. 11 and 12 show that the technique cannot in the present cases be used to determine conclusively the interatomic potential.

The differences between the line shapes simulated for Si using the DMol and ZBL potentials (Fig. 12) are not as large as in the case of Ti. This is due to the fact that the potential curves cross each other inside the potential region probed in this work (340–5 eV): below 45 eV the ZBL is stronger and above 45 eV the DMol is stronger. Also because the lifetime of the nuclear state of ^{29}Si is longer than that of ^{49}Ti, the fine structure in line shapes is not so pronounced as in the line shapes of Ti. Thus the differences caused by different Si potentials are not as clear as in the corresponding case of Ti.

E. Effect of lattice defects

The fact that in the simulations the recoiling atoms leave from lattice sites and slow down in perfect crystals means that the effect of possible lattice defects were ignored. However, the concentrations of intrinsic defects are at the studied temperatures so low that this was justified. The slowing-down process itself creates damage in an approximate volume of $15 \times 10 \times 10$ Å^3. This damage can also be ignored in the simulations as long as the damaged areas do not overlap. In a typical GRID measurement for ^{49}Ti with a Ti target[20] one uses a thermal neutron flux of 5×10^{14} cm^{-2} s^{-1}, in which the neutron capture cross section and target mass and volume are 7.8 b, 14.6 g, and 3.2 cm^3, respectively. Then an irradiation time of 48 days would be needed to create overlap of damaged areas, provided that no correction of the damage takes place.

V. CONCLUSIONS

The dependence of the slowing down of energetic atoms on the crystal structure and the initial recoil direction with respect to crystal axes has been studied with molecular-dynamics simulations. The effect of the crystal structure on the slowing down of low-energy Ti and Si recoils in single crystal Ti and Si samples, respectively, is clearly exhibited in the simulated GRID γ-ray line shapes. The fine structure of the line shapes, depending on the distribution of the projections of the recoil velocities along the direction of the detector, depends strongly on the angular distribution of the recoil velocity, and on the distance the recoiling atoms traverse. This means that in the crystal the product of the initial recoil velocity and nuclear lifetime has to correspond to 2–3 interatomic distances.

The GRID line shapes are found to show a complicated fine structure which is sensitive to the interatomic potential used in the simulations. However, it is pointed out that in the aim of producing the experimentally observed line shapes the change in the potential can not be compensated by the change in the lifetime of the nuclear level. This gives better possibilities in planing GRID measurements to study the interatomic potential in a bulk matter than was possible in previous measurements.[10]

ACKNOWLEDGMENTS

This work was supported by the Academy of Finland. The work has been made possible by computer resources from the Center of Scientific Computing, Espoo, Finland.

[1] H. G. Börner, J. Phys. G **14**, S143 (1988).
[2] H. G. Börner and J. Jolie, J. Phys. G **19**, 217 (1993).
[3] H. G. Börner, J. Jolie, F. Hoyler, S. J. Robinson, and M. S. Dewey, Phys. Lett. B **215**, 45 (1988).
[4] E. G. Kessler, G. L. Greene, M. S. Dewey, R. D. Deslattes, H. G. Börner, and F. Hoyler, J. Phys. G **14**, S167 (1988).
[5] M. S. Dewey, E. G. Kessler, G. L. Greene, R. D. Deslattes, H. G. Börner, and J. Jolie, Nucl. Instrum. Methods A **284**, 151 (1989).
[6] M. Robinson and I. Torrens, Phys. Rev. B **9**, 5008 (1974).
[7] D. E. Harrison, Jr., Crit. Rev. Solid State Sci. **14**, 1 (1988).
[8] A. Kuronen, J. Phys. Condens. Matter **3**, 1363 (1991).
[9] A. Kuronen, J. Keinonen, H. G. Börner, J. Jolie, and S. Ulbig, Nucl. Phys. **A549**, 59 (1992).
[10] J. Keinonen, A. Kuronen, P. Tikkanen, H. G. Börner, J. Jolie, S. Ulbig, E. G. Kessler, R. M. Nieminen, M. J. Puska, and A. P. Seitsonen, Phys. Rev. Lett. **67**, 3692 (1991).
[11] K.-H. Heinig and D. Janssen (unpublished).
[12] T. W. Burrows, Nucl. Data Sheets **48**, 569 (1986).
[13] P. M. Endt, Nucl. Phys. **A521**, 1 (1990).
[14] S. Raman, E. T. Turney, J. W. Starner, and J. E. Lynn, Phys. Rev. C **46**, 972 (1992).
[15] R. S. Smith and D. E. Harrison, Jr., Comput. Phys. **Sep/Oct 1989**, 68 (1989).
[16] L. A. Girifalco and W. G. Weizer, Phys. Rev. **114**, 687 (1959).
[17] J. Keinonen, A. Kuronen, K. Nordlund, R. M. Nieminen, and A. P. Seitsonen (unpublished).
[18] A. M. Mazzone, Philos. Mag. Lett. **60**, 131 (1989).
[19] J. F. Ziegler, J. P. Biersack, and U. Littmark, *The Stopping and Range of Ions in Matter* (Pergamon, New York, 1985), Vol. 1.
[20] S. Ulbig, Ph.D. thesis, University of Göttingen, 1991.

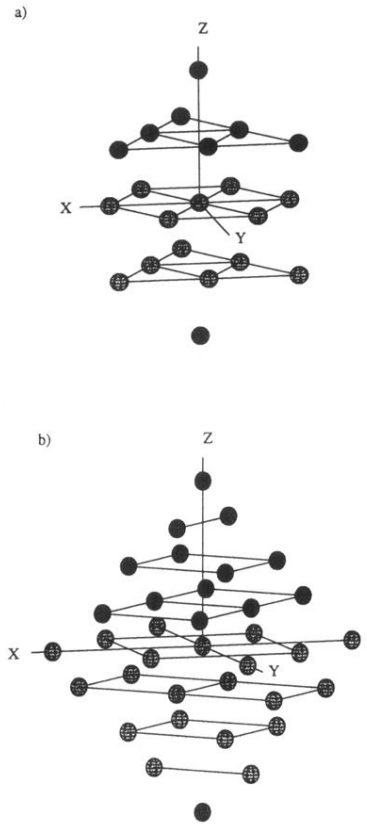

FIG. 1. (a) Nearest neighbors in the hcp lattice. Due to the different environments of successive layers the other sublattice can be formed by rotating the figure around the z axis through 60°. (b) Nearest neighbors in the diamond lattice. The other sublattice can be formed by rotating the figure around the z axis through 90°.

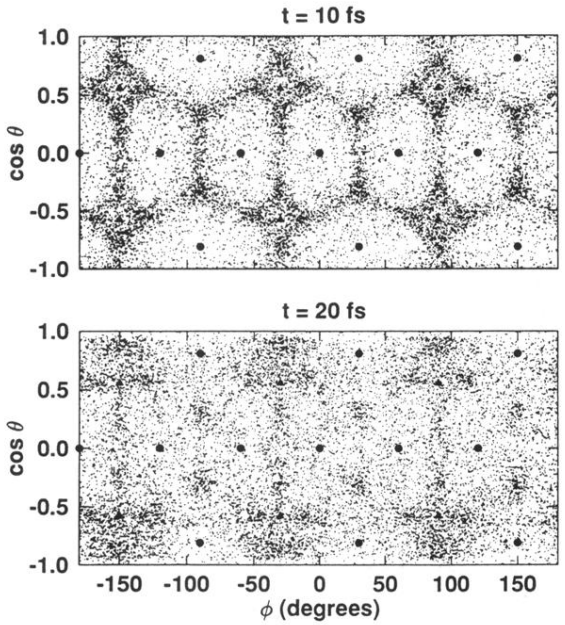

FIG. 3. Simulated angular distribution of the recoil velocities of ^{49}Ti atoms recoiling in single-crystal Ti 10 and 20 fs after the start of the recoil event. The recoiling atom was always from the same sublattice of the hcp structure. The directions of the nearest (circles) and second-nearest (triangles) neighbors are shown. The other sublattice results can be formed by shifting the pattern 60° along the ϕ axis. The EMT potential was used in the simulation.

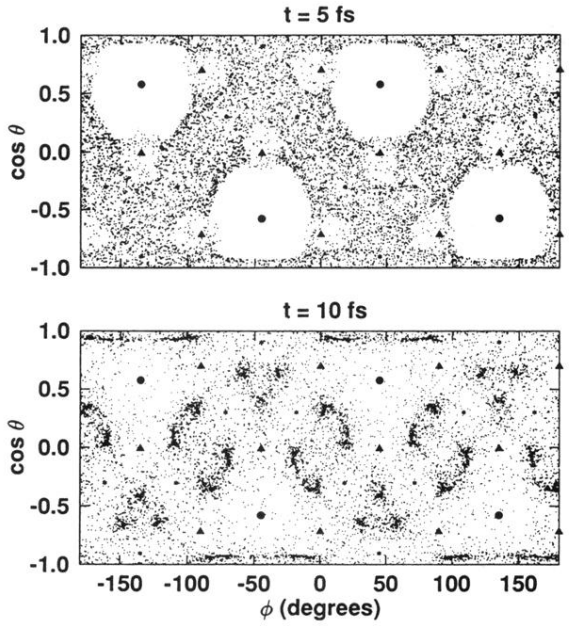

FIG. 4. Simulated angular distribution of the recoil velocities of ^{29}Si atoms recoiling in single-crystal Si 5 and 10 fs after the start of the recoil event. The recoiling atom was always from the same sublattice of the diamond structure. Also shown are the directions of the nearest (circles), second-nearest (triangles), and third-nearest (asterisks) neighbors. The other sublattice results can be obtained by shifting the pattern 90° along the ϕ axis. The DMol potential was used in the simulation.